Journal of Alloys and Compounds 498 (2010) 37–41

Contents lists available at ScienceDirect

Journal of Alloys and Compounds

journal homepage: www.elsevier.com/locate/jallcom

# High-density $NiTiO_3/TiO_2$ nanotubes synthesized through sol–gel method using well-ordered $TiO_2$ membranes as template

Dong Fang[a], Kelong Huang[a,*], Suqin Liu[a], Zhiping Luo[b], Xiaoxia Qing[a], Qiguang Zhang[a]

[a] College of Chemistry & Chemical Engineering, Central South University, Changsha 410083, People's Republic of China
[b] Microscopy and Imaging Center, Texas A&M University, College Station, TX 77843, USA

ARTICLE INFO

*Article history:*
Received 5 September 2009
Received in revised form 16 February 2010
Accepted 21 February 2010
Available online 3 March 2010

*Keywords:*
Nanotube
Nanofabrication
Sol–gel process
$TiO_2$
$NiTiO_3$

ABSTRACT

Free-standing and well-ordered $TiO_2$ membranes were prepared by two-step anodization in $F^-$-containing ethylene glycol electrolytes at voltage of 60 V. It was found that the ordering of $TiO_2$ membranes was significantly improved after the second anodization process. The initially closed bottom side of $TiO_2$ membranes was opened through chemical etching to obtain two-end opened $TiO_2$ membranes. Using the two-end opened membranes as template, dense $NiTiO_3/TiO_2$ nanotubes were successfully prepared for the first time by a sol–gel method. The microstructure and morphologies of the samples were characterized by scanning and the transmission electron microscopy techniques.



## 1. Introduction

The $TiO_2$ nanotube materials have been widely studied due to their potential technological applications in lithium batteries [1,2], solar cells [3], and photocatalysis [4]. The $TiO_2$ nanotube growth on titanium (Ti) under anodic bias in electrolytes has been an object for over a decade [5]. At least two different electrolytes were reported so far, the aqueous electrolyte [6–8] and non-aqueous organic electrolyte [9] respectively, yielding two distinguishable morphologies [10–12]. The mechanisms of the nanotubes formation have also been discussed previously by Yasuda et al. [13,14].

Towards the application of nanomaterials, as porous alumina membranes have relatively regular structure with concentrated size distributions in pore diameter and interpore spacing, they have been utilized as nanofilters to selectively filtrate nanomaterials, drug separation, as well as a host or template for nanodevices, such as magnetic, electronic, or optoelectronic devices [15]. On the other hand, well-ordered anodic titanium dioxides (ATO) also have potential applications as the porous alumina membranes. In addition, fabricating well-ordered ATO would provide clues for better understanding the formation mechanism of the anodization [16]. Efforts have been made to fabricate highly ordered nanoporous $TiO_2$ membranes by several groups [17–19].

Recently, ternary oxides containing titanium and transition metals, such as $MTiO_3$ (M = Ni, Pb, Fe, Co, Cu and Sr), are increasingly recognized as chemical or electrical materials because of their outstanding catalytic, ferroelectric, piezoelectric, pyroelectric, dielectric, and photoelectric properties [20–23]. Several methodologies, such as sol–gel [24], hydrothermal [25], sputtering [26], co-precipitations [27], solid-state reactions [28], and polymeric precursor method [29] have been proposed for synthesising crystalline $MTiO_3$ powders. While, $MTiO_3$ fabricated by these methods usually require complex equipments and complicated operation procedures. On the other hand, the traditional way to produce $MTiO_3$ using solid reaction produces large $MTiO_3$ particles with uncontrollable morphologies, due to their inherent problems such as high reaction temperature and heterogeneous solid phase reactions.

In the present work, we first attempt to fabricate well-ordered free-standing ATO membranes with ideal hexagonal ordering using the two-step anodization process. Second, two-end opened ATO membranes are obtained by chemical etching. Finally, high-density $NiTiO_3/TiO_2$ nanotubes are prepared by the sol–gel method on the two-end opened ATO template. Electron microscopic characterizations confirm the formation of $NiTiO_3/TiO_2$ nanostructures.

## 2. Experimental procedures

### 2.1. Preparation of $TiO_2$ nanotubes

Titanium (Ti) foils (99.6% purity, 0.3 mm thick) were degreased by sonication in acetone, isopropanol and methanol, respectively. This procedure was followed

* Corresponding author.
*E-mail addresses:* klhuang@mail.csu.edu.cn (K. Huang), luo@mic.tamu.edu (Z. Luo).

0925-8388/$ – see front matter © 2010 Elsevier B.V. All rights reserved.
doi:10.1016/j.jallcom.2010.02.150

by rinsing with deoinized water and then drying in a nitrogen stream. The electrochemical setup consisted of a two-electrode configuration with graphite as counter electrode. All anodization experiments were carried out at room temperature in glycol solution. The anodic titania was grown at a voltage of 60 V for 48 h. Afterwards, the whole samples were transferred into 95% of ethanol solution for ultrasonic agitation for several minutes. After removing the anodic oxide layers using ultrasonic agitation, the textured Ti substrate was anodized again under the same conditions as the first anodizing step.

### 2.2. Preparation of $NiTiO_3/TiO_2$ nanotubes

Before using free-standing ATO membrane, the bottom closed side of the membrane was chemically etched using a 5 wt% $NH_4F$-1 M $H_2SO_4$ solution for 15 min, to obtain two-end opened ATO membrane [30]. Then the two-end opened ATO membrane was immersed into the sol for 10 h under relative vacuum ambience. For the sol fabricating, nickel nitrate was used as the cationic source, and citric acid and alcohol as the monomers to form the polymeric matrix. Therefore, the $Ni(NO_3)_2$ was added to dissolve into a mixture of citric acid and alcohol solution, with molar ratio of $Ni^{2+}$ to citric acid as 1:2, and then the solution was heated at 70 °C to distill out excess alcohol. Finally, the two-end opened ATO membrane was placed in a furnace and annealed at 450 °C for 2 h under atmosphere.

### 2.3. Materials characterization

The samples were characterized by scanning electron microscopy (SEM, JSM-6360LV) and transmission electron microscope (TEM, JEM-2100). For the SEM, a thin Au layer (~3 nm) was evaporated on the sample surface to form a conductive film for the observation. For the TEM, a small piece of the template with $NiTiO_3$ nanoparticles was immersed into 1 ml water, which was broken into fine pieces using ultrasonication, and then a drop of the solution was placed onto a Cu grid covered with carbon support film. Quantitative measurements of electron diffraction (ED) intensities were made using ELD program [31,32] in Crisp package [33], and the simulations of powder ED patterns were performed using the Reflex module in Materials Studio, Version 5.0, by Accelrys.

## 3. Results and discussion

In the initial stage of the anodization, the degree of the ordering at the surface of the ATO is low, since the surface of the starting material is relatively rough at the micrometer scale. As a result, holes develop randomly. To improve the ATO ordering on the surface, two-step anodization is exercised. This process involves two separate anodization procedures, as sketched in Fig. 1. Starting form the Ti film with rough top surface (Fig. 1a), the first anodization process is a long-period anodization to form the highly ordered dimple configuration at the $TiO_2$/Ti interface using the electrochemical anodization of Ti foil at 60 V (Fig. 1b). Subsequently, the textured Ti substrate was obtained after removing the ATO membrane using ultrasonic agitation in 95% of ethanol solution (Fig. 1c). Then the textured Ti substrate was anodized again under conditions identical to the first anodizing step, in which a way an ordered holes array throughout the entire oxide layer was generated in this process (Fig. 1d). Using ultrasonic agitation, the free-standing and well-ordered ATO membrane, with ideally hexagonal ordering, could be peeled off from the Ti substrate.

In the ATO membrane prepared by the first anodization, as shown in the SEM image of the top surface in Fig. 2(a), the ordering areas are limited, with evident gaps exist between them, and the degree of hexagonal ordering is also limited. Fig. 2(b) shows the Ti substrate after removing the $TiO_2$ membrane, which exhibits relatively flat dimpled surface, acting as the starting material for the second anodization.

By the second anodization, free-standing and well-ordered ATO membrane was produced, as shown in Fig. 3. Its average pore diameter ($d_p$) is about 115 nm as measured from its top surface (Fig. 3a), and the length of the membrane is about 158.3 μm as revealed from the cross-sectional view in Fig. 3(b). Fig. 3(c) is the SEM image of the bottom side of the film, depicting that the nanotubes are completely closed at this end. Fig. 3(d) shows an image of the free-standing well-ordered ATO membrane taken using an ordinary digital camera, with the dimensions of the membrane about $2.0 \times 2.0\ cm^2$.

In order to fabricate $NiTiO_3$ inside the well-ordered ATO membrane, as shown in Fig. 4, the well-ordered ATO membrane (Fig. 4a) was soaked in 0.5 wt% $NH_4F$-1 M $H_2SO_4$ solution to obtain the two-end opened ATO membrane (Fig. 4b) [30]. Afterwards, the two-end opened ATO membrane was immersed in the sol under relative vacuum ambience so that the sol could get into the tube during this process (Fig. 4c). The membrane was then taken out from

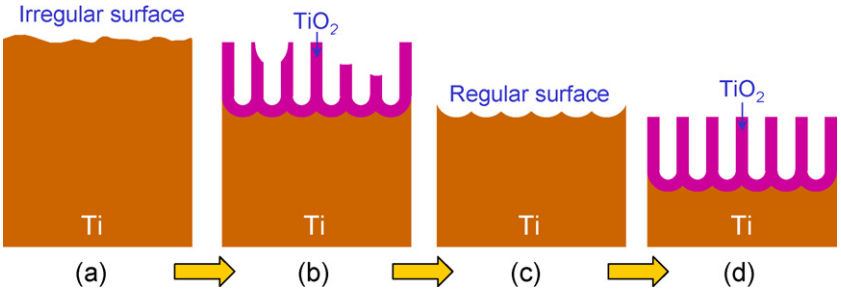


**Fig. 1.** Two-step anodization process. (a) Starting material with irregular surface; (b) formation of $TiO_2$ nanotubes after the first anodization; (c) regular dimpled surface after removing the $TiO_2$ nanotubes by the first anodization; (d) formation of well-ordered $TiO_2$ nanotubes after the second anodization.

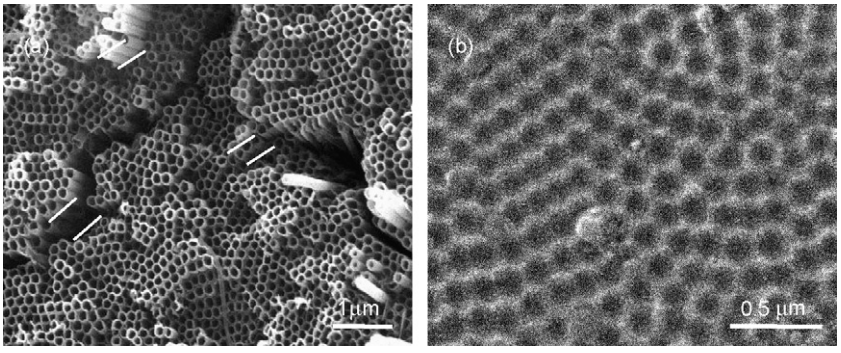


**Fig. 2.** SEM images of (a) top surface of porous $TiO_2$ membrane formed by the first-step anodization, and (b) titanium substrate surface after removing the $TiO_2$ membrane.

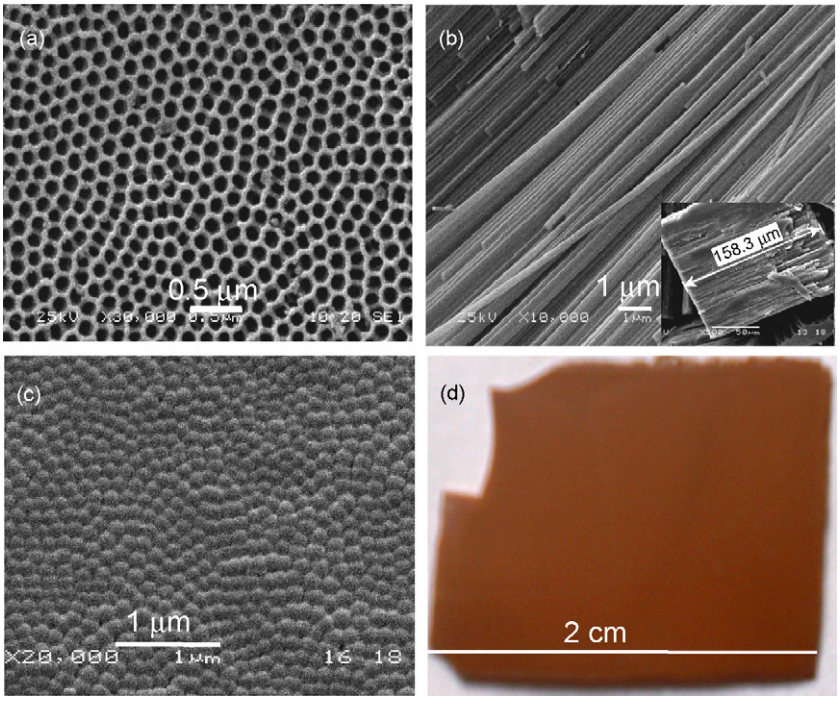


**Fig. 3.** SEM images of the well-ordered ATO membrane by two-step anodization along the top view (a), cross-sectional view (b), and bottom view (c). The inset in (b) shows the thickness of the membrane. The image of the membrane in (d) is taken by an ordinary digital camera, showing the planar dimensions of the membrane.

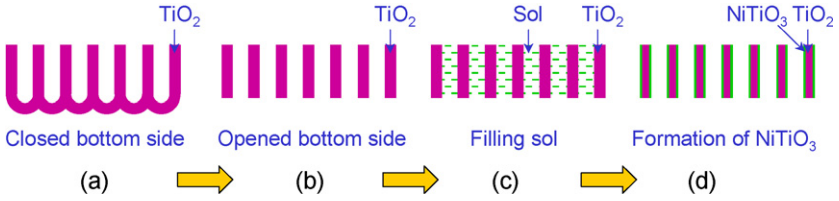


**Fig. 4.** Synthesizing $NiTiO_3$ process. (a) Starting material of the well-ordered ATO membrane produced by two-step anodization; (b) opening the bottom side by chemical etching; (c) filling the two-end opened membrane with sol; (d) formation of $NiTiO_3$.

the sol, and washed in ethanol. Finally, the sample was annealed in air to obtain $NiTiO_3/TiO_2$ nanotube membrane (Fig. 4d). We observed that the final $NiTiO_3/TiO_2$ nanotube membrane exhibited light green colour.

Fig. 5(a) shows the SEM image of a transverse section of the as-prepared $NiTiO_3/TiO_2$ membrane, which was made by cutting the sample along the transverse direction using a blade. The energy dispersive X-ray (EDX) spectrum of the $NiTiO_3/TiO_2$ nanotubes is shown in Fig. 5(b), with the evidence of Ni and the Ti/Ni atomic ratio is about 11:1.

Fig. 6(a) and (b) is typical TEM images of a bundle and a single $NiTiO_3/TiO_2$ nanotube, respectively. They still retain their structural integrity on the TEM grids after the ultrasonication process in the TEM sample preparation. The HRTEM image in Fig. 6(c) is taken from the single nanotube in Fig. 6(b). Most of the areas are identified as $TiO_2$ nanocrystals with the anatase phase (tetragonal

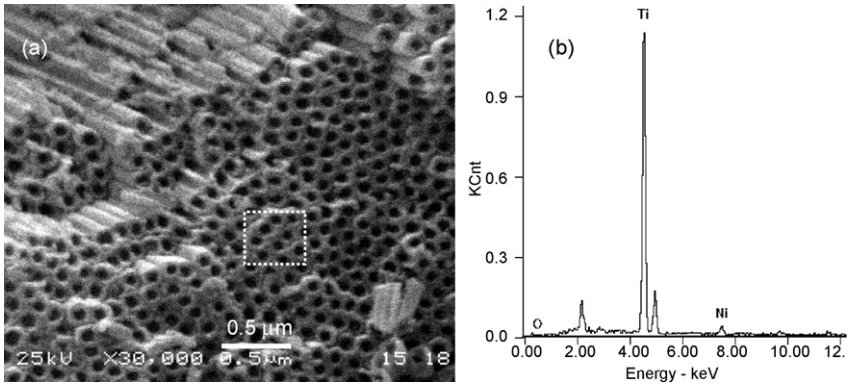


**Fig. 5.** Transverse section view of SEM image (a) and EDX spectrum (b) of $NiTiO_3/TiO_2$ nanotube.

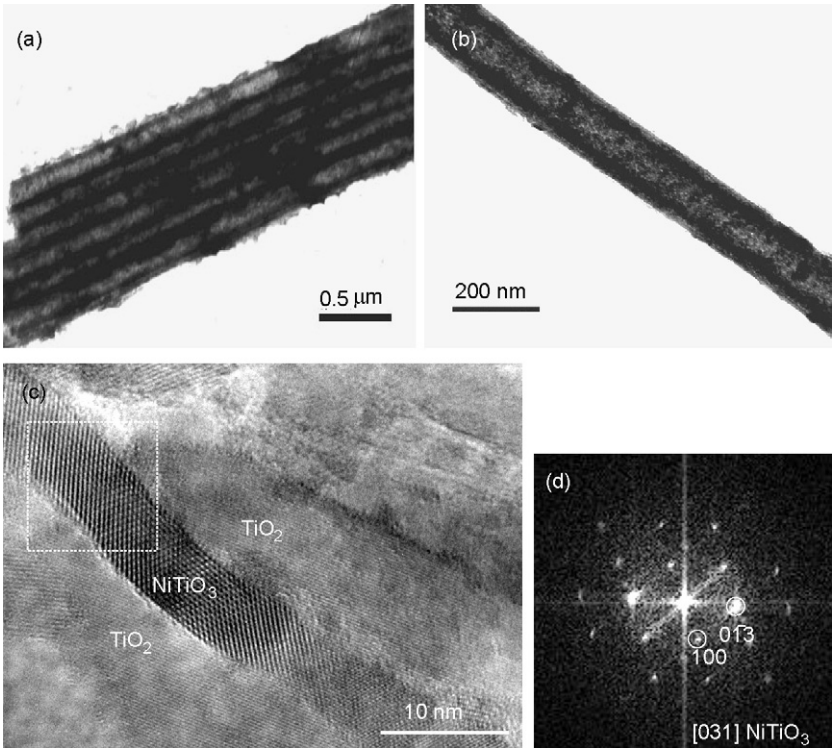


**Fig. 6.** TEM images showing a bundle (a) and a single $NiTiO_3/TiO_2$ nanotubes (b). The HRTEM image in (c) is taken from the single nanotube in (b), whose framed area gives the FT pattern in (d) showing the $NiTiO_3$ ilmenite structure.

structure, with space group of $I4_1/amd$, and lattice parameters of $a = 0.378479$ nm, $c = 0.951237$ nm) [34]. However, the band shaped phase in Fig. 6(c) exhibits clearly a different structure with larger lattice spacing. A Fourier transformation (FT) pattern from the framed area in Fig. 6(c) is given in Fig. 6 (d), which confirms the $NiTiO_3$ ilmenite phase (rhombohedral structure, with space group of $R\bar{3}c$, and lattice parameters of $a = 0.50321$ nm, $c = 1.37924$ nm) [35].

A further confirmation of the ilmenite structure is made by quantitative electron diffraction analysis over larger areas. Fig. 7(a) and (c) are two ED patterns taken from different regions, where Fig. 7(a) shows the strongest reflections at the innermost position, while Fig. 7(c) shows the innermost reflections are weak, while the second innermost reflections are the strongest. Fig. 7(b) and (d) is the reflection intensity profiles starting from the center direct beam, resulted using the program ELD [31,32] and then processed using Reflex in Materials Studio. The backgrounds were calculated using Reflex module, as shown in Fig. 7(b) and (d), respectively. After subtracting the background, the two intensity profiles are shown in Fig. 7(e), together with simulated powder ED patterns of the $TiO_2$ anatase, $NiTiO_3$ ilmenite, and NiO (face-centered cubic structure, with space group of $Fm\bar{3}m$, and lattice parameter $a = 0.41684$ nm) structures. From the ED pattern simulations, it is seen that the first peak (1 0 1) of $TiO_2$ anatase is the strongest that is consistent to the previous work [36,37], while the first peak (1 0 $\bar{2}$) of $NiTiO_3$ ilmenite is weak but its second peak,

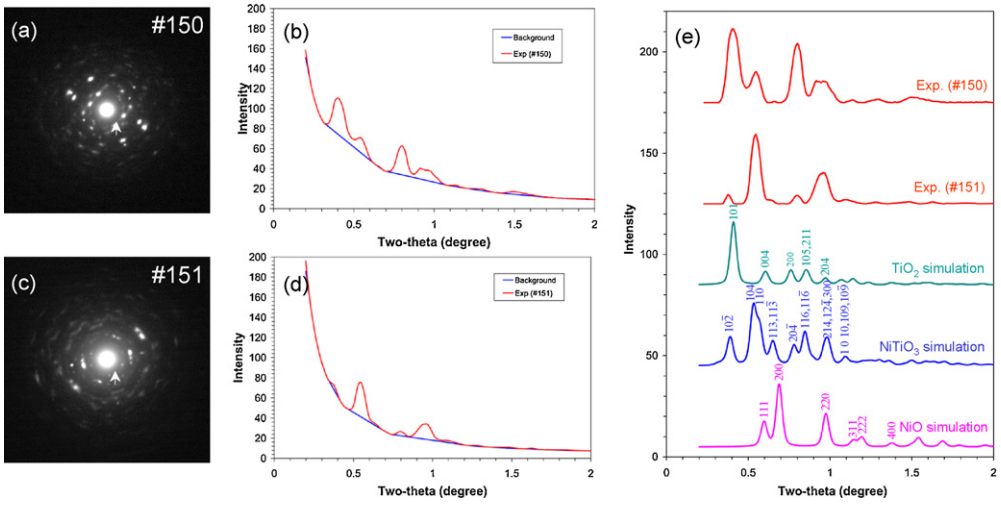


**Fig. 7.** Quantitative analysis of ED patterns taken from two different areas (a and c), with their intensity profiles given in (b) and (d), respectively. After subtracting the background, the intensity profiles are given in (e), compared with simulated powder ED patterns of $TiO_2$ anatase, $NiTiO_3$ ilmenite, and NiO structures.

composed of (1 0 4) and (1 1 0), is the strongest. The first two reflections from the NiO phase locate at higher angles. As compared to these simulations, it is found that the ED pattern #150 in Fig. 7(a) contains reflections from both $TiO_2$ anatase (major one) and $NiTiO_3$ ilmenite (minor one), while the ED pattern #151 in Fig. 7(c) contains reflections predominately from the $NiTiO_3$ ilmenite phase. None of these two patterns exhibit the evidence of the NiO structure, whose strongest peak (2 0 0) does not appear in their intensity profiles.

From the results, it is evident that the $NiTiO_3/TiO_2$ nanotubes were successfully fabricated.

## 4. Conclusions

In summary, we have fabricated free-standing and well-ordered ATO membrane by the two-step anodization of Ti substrate in ethylene glycol/$NH_4F$ electrolytes, under the condition of 60 V. The quality of the structure, in terms of assembly defects, was greatly improved after the second anodization. The fabricated dense porous material is the first example of $NiTiO_3/TiO_2$ combination among several other systems, such as $PbTiO_3$ [23,25], $SrTiO_3$ [24], $BaTiO_3$ [20,24], etc., prepared so far. The sol–gel method using the two-end opened ATO membrane as template was a facile possible way to fabricate the $NiTiO_3/TiO_2$ compound nanotubes, which opens a new avenue to prepare these composite materials by the sol–gel method. These materials have great potentials to find applications if they are associated with high porosity, optical quality, high accessibility and high surface-to-volume ratio.

## Acknowledgements

This work was supported by the National Natural Science Foundation of China (no. 50772133, no. 20976016), Innovation Projects for Undergraduates of Center South University (no. LA09014), and Innovation Projects for Graduates of Hunan Province (no. CX2009B047). The program Reflex module in Materials Studio for simulating powder electron diffraction pattern was provided by Laboratory for Molecular Simulation, Department of Chemistry, Texas A&M University.

## References

[1] J. Xu, C. Jia, B. Cao, W.F. Zhang, Electrochem. Acta 52 (2007) 8044–8047.
[2] D. Fang, K.L. Huang, S.Q. Liu, Z.J. Li, J. Alloys Compd. 464 (2008) L5–L9.
[3] C.J. Lin, W.Y. Yu, Y.T. Lu, S.H. Chien, Chem. Commun. 45 (2008) 6031–6033.
[4] N.K. Shrestha, J.M. Macak, F. Schmidt-Stein, R. Hahn, C.T. Mierke, B. Fabry, P. Schmuki, Angew. Chem. Int. Ed. 48 (2009) 969–972.
[5] V. Zwilling, E. Darque-Ceretti, A. Boutry-Forveille, D. David, M.Y. Perrin, M. Aucouturier, Surf. Interface Anal. 27 (1999) 629–637.
[6] D. Gong, C.A. Grimes, O.K. Varghese, W.C. Hu, R.S. Singh, Z. Chen, E.C. Dickey, J. Mater. Res. 16 (2001) 3331–3334.
[7] J.M. Macak, H. Tsuchiya, P. Schmuki, Angew. Chem. Int. Ed. 44 (2005) 2100–2102.
[8] D. Fang, K.L. Huang, S.Q. Liu, J.H. Huang, J. Braz. Chem. Soc. 19 (2008) 1059–1064.
[9] M. Paulose, K. Shankar, S. Yoriya, H.E. Prakasam, O.K. Varghese, G.K. Mor, T.A. Latempa, A. Fitzgerald, C.A. Grimes, J. Phys. Chem. B 110 (2006) 16179–16184.
[10] J.M. Macak, K. Sirotna, P. Schmuki, Electrochim. Acta 50 (2005) 3679–3684.
[11] H. Tsuchiya, J.M. Macak, L. Muller, J. Kunze, F. Muller, P. Greil, S. Virtanen, P. Schmuki, J. Biomed. Mater. Res. A 77 (2006) 534–541.
[12] K. Shankar, G.K. Mor, H.E. Prakasam, S. Yoriya, M. Paulose, O.K. Varghese, C.A. Grimes, Nanotechnology 18 (2007), 065707 (11).
[13] K. Yasuda, J.M. Macak, S. Berger, A. Ghicov, P. Schmuki, J. Electrochem. Soc. 154 (2007) C472–C478.
[14] K. Yasuda, P. Schmuki, Electrochim. Acta 52 (2007) 4053–4061.
[15] M. Lai, D.J. Riley, J. Colloid Interface Sci. 323 (2008) 203–212.
[16] Z.X. Su, W.Z. Zhou, Adv. Mater. 20 (2008) 3663–3667.
[17] J.M. Macak, S.P. Albu, P. Schmuki, Phys. Status Solidi (RRL) 1 (2007) 181–183.
[18] G.G. Zhang, H.T. Huang, Y.H. Zhang, H.L.W. Chan, L.M. Zhou, Electrochem. Commun. 9 (2007) 2854–2858.
[19] Y. Shin, S. Lee, Nano Lett. 8 (2008) 3171–3173.
[20] K.J. Choi, M. Biegalski, Y.L. Li, A. Sharan, J. Schubert, R. Uecker, P. Reiche, Y.B. Chen, X.Q. Pan, V. Gopalan, L.Q. Chen, D.G. Schlom, C.B. Eom, Science 306 (2004) 1005–1009.
[21] C.H. Ahn, K.M. Rabe, J.M. Triscone, Science 303 (2004) 488–491.
[22] D.D. Fong, G.B. Stephenson, S.K. Streiffer, J.A. Eastman, O. Auciello, P.H. Fuoss, C. Thompson, Science 304 (2004) 1650–1653.
[23] J.M. Macak, C. Zollfrank, B.J. Rodriguez, H. Tsuchiya, M. Alexe, P. Greil, P. Schmuki, Adv. Mater. 21 (2009) 1–5.
[24] J. Moreno, J.M. Dominguez, A. Montoya, L. Vicente, T. Viveros, J. Mater. Chem. 5 (1995) 509–512.
[25] Y. Yang, X. Wang, C. Zhong, C. Sun, L. Li, Appl. Phys. Lett. 92 (2008) 122907–122910.
[26] Z. Pan, S.K. Donthu, N. Wu, S. Li, V.P. Dravid, Small 2 (2006) 274–280.
[27] Y.K. Sharma, M. Kharkwal, S. Uma, R. Nagarajan, Polyhedron 28 (2009) 579–585.
[28] K. Sreedhar, A. Mitra, J. Am. Ceram. Soc. 83 (2000) 418–420.
[29] K.P. Lopesa, L.S. Cavalcantea, A.Z. Simõesb, J.A. Varelab, E. Longob, E.R. Leitea, J. Alloys Compd. 486 (2009) 327–332.
[30] D. Fang, K.L. Huang, S.Q. Liu, D.Y. Qin, Electrochem. Commun. 11 (2009) 901–904.
[31] X.D. Zou, Y. Sukharev, S. Hovmoller, Ultramicroscopy 49 (1993) 147–158.
[32] X.D. Zou, Y. Sukharev, S. Hovmoller, Ultramicroscopy 52 (1993) 436–444.
[33] S. Hovmoller, Ultramicroscopy 41 (1992) 121–135.
[34] J.K. Burdett, T. Hughbanks, G.J. Miller, J.W. Richardson, J.V. Smith, J. Am. Chem. Soc. 109 (1987) 3639–3646.
[35] R.P. Liferovich, R.H. Mitchell, Phys. Chem. Miner. 32 (2005) 442–449.
[36] T.E. Weirich, M. Winterer, S. Seifried, H. Hahn, H. Fuess, Ultramicroscopy 81 (2000) 263–270.
[37] T.E. Weirich, M. Winterer, S. Seifriedb, J. Mayer, Acta Cryst. A 58 (2002) 308–315.